Penternary Wurtzitic Nitrides $Li_{1-x}Zn_xGe_{2-x}Ga_xN_3$: Powder Synthesis, Crystal Structure, and Potentiality as a Solar-Active Photocatalyst

Takayuki Suehiro,[*,†] Masataka Tansho,[‡] Akio Iwanade,[§] Toru Ishigaki,[#] and Naoki Ohashi[†]

[†]*Electro-Ceramics Group, Research Center for Electronic and Optical Materials, National Institute for Materials Science, 1-1 Namiki, Tsukuba 305-0044, Japan*

[‡]*Solid-State NMR Group, Center for Basic Research on Materials, National Institute for Materials Science, 3-13 Sakura, Tsukuba 305-0003, Japan*

[§]*Materials Fabrication and Analysis Platform, Research Network and Facility Services Division, National Institute for Materials Science, 1-1 Namiki, Tsukuba 305-0044, Japan*

[#]CROSS Neutron Science and Technology Center, 162-1 Shirakata, Tokai, Naka, Ibaraki 319-1106, Japan

*Corresponding author. E-mail: suehiro.takayuki@nims.go.jp.

ABSTRACT:

We have developed a new penternary wurtzitic nitride system $Li_{1-x}Zn_x$-$Ge_{2-x}Ga_xN_3$ ($0 \leq x \leq 1$) by hybridizing $LiGe_2N_3$ and $ZnGeGaN_3$. Fairly stoichiometric fine powder samples were synthesized by the reduction–nitridation process at 900°C. While the end member $LiGe_2N_3$ possessed a relatively large band gap of 4.16 eV, the band gap of the developed penternary system varied in a broad range of 3.81–3.10 eV, showing promising responsivity to the solar spectrum. The crystal structure of $LiGe_2N_3$ was precisely determined by time-of-flight neutron powder diffraction for the first time, revealing the complete ordering of Li and Ge in the $Cmc2_1$ structure. The structural evolution from the completely ordered $LiGe_2N_3$ to the fully disordered $ZnGeGaN_3$ was quantitatively analyzed by Rietveld refinement based on a partially disordered $Cmc2_1$ model, and the obtained results were also supported by ^{71}Ga solid-state NMR spectroscopy. The synthesized $Li_{1-x}Zn_xGe_{2-x}Ga_xN_3$ powder samples exhibited photocatalytic activities for the water reduction and oxidation reactions under solar-light irradiation, with the H_2 evolution rate of 0.3–59.0 μmol/h and the O_2 evolution rate of 3.1–296.2 μmol/h, depending on the composition. Stable solar hydrogen generation of up to 48 h was demonstrated by the $x = 0.80$ sample, with the total amount of H_2 evolved over 1.6 mmol and the external quantum efficiency of 2.1%.

1 Introduction

Mutinary wurtzitic nitrides have attracted considerable attention in recent years, owing to their potentiality for optoelectronic, photovoltaic, photocatalytic, electrochemical, and spintronic applications.[1−24] Most of them synthesized experimentally to date are restricted to ternary systems such as II–IV–N_2 and II_2–V–N_3, which essentially possess no compositional flexibility and thus, limited tunability for physical properties, unless controlling the cation (dis)order or alloying (solid-solution formation).

We explored the solid-solution formation between $ZnGeN_2$ and GaN for the first time, and established a quaternary wurtzitic nitride system $Zn_{1-x}Ge_{1-x}Ga_{2x}N_2$.[17] The band gap of $Zn_{1-x}Ge_{1-x}Ga_{2x}N_2$ showed an abrupt decrease from 3.42 eV for $x = 0$ to the visible-light range of 3.05–3.02 eV for $x = 0.10$–0.50, depending little on the value of x. The observed unusual reduction of the band gap was attributed to the predicted staggered (type-II) band offset and the minimal lattice mismatch between $ZnGeN_2$ and GaN.[25−27] Refinements of the crystal structure and ^{71}Ga solid-state NMR spectroscopy indicated that cation ordering in the octet-rule-preserving structure of $ZnGeN_2$ ($Pna2_1$) nearly disappears at $x = 0.10$, transitioning to a fully disordered $P6_3mc$ phase when $x \geq 1/3$. The synthesized $Zn_{1-x}Ge_{1-x}Ga_{2x}N_2$ showed photocatalytic activity for water splitting reactions, achieving H_2 evolution rates between 2.8 and 3.6 μmol/h and high O_2 evolution rates of 100.4 to 126.6 μmol/h under visible light irradiation with wavelengths greater than 400 nm. Jayatunga and Lambrecht et al.[28] predicted potential crystal structures and band structures for the $Zn_{1-x}Ge_{1-x}Ga_{2x}N_2$ system at $x = 0.5$ through first-principles calculations. They found that, contrary to expectations, the band gaps of two simulated octet-rule-preserving superlattices ($Pmn2_1$, $P1n1$) were marginally larger than

those of the end members, whereas another superlattice that violated the octet rule and was energetically unfavorable exhibited a reduced band gap. Their findings suggested that the marked band-gap narrowing observed in our earlier study might not be due to the anticipated type-II band alignment, but rather to the cation disorder caused by Ga incorporation. We further investigated the $Zn_{1-x}Ge_{1-x}Ga_{2x}N_2$ system with previously unexamined low-Ga concentrations of $x = 0.02$ and 0.05, to clarify the transitionary optical and structural evolution induced by Ga incorporation.[8] Detailed analyses using time-of-flight (TOF) neutron powder diffraction and high-field ^{71}Ga NMR spectroscopy showed that the markedly reduced band gap attained in $Zn_{1-x}Ge_{1-x}Ga_{2x}N_2$ is mainly due to the cation disorder. With the synthesized $x = 0.02$ sample, photocatalytic water reduction of up to 5 days was performed under simulated solar-light irradiation, with an average H_2 evolution rate of 23.4 μmol/h.

In the current work, we developed a new penternary nitride system $Li_{1-x}Zn_xGe_{2-x}$-Ga_xN_3 by hybridizing ternary and quaternary wurtzitic nitrides, $LiGe_2N_3$ and $ZnGeGaN_3$. The existence of $LiGe_2N_3$ has been reported as early as 1974,[29] whereas its physicochemical properties have not been explored up to now, except for the crystal structure determined by X-ray diffraction (XRD) and optical absorption properties reported by Häusler et al.[30] While $ZnGeGaN_3$ corresponds to $x = 1/3$ in the $Zn_{1-x}Ge_{1-x}Ga_{2x}N_2$ system and should be regarded as $Zn_{1/3}Ge_{1/3}Ga_{1/3}N$ from the crystallographic point of view, its formula will be represented as "$ZnGeGaN_3$" hereafter for convenience. The synthesis of $Li_{1-x}Zn_x$-$Ge_{2-x}Ga_xN_3$ fine powder samples was established by the gas-reduction–nitridation (GRN) process, and integrity of the designed composition was confirmed thoroughly by chemical analyses. The formation of the solid solution and the resulting structural evolution

were examined by the Rietveld refinement and ^{71}Ga solid-state NMR spectroscopy. The synthesized $Li_{1-x}Zn_xGe_{2-x}Ga_xN_3$ exhibited promising sensitivity to the solar spectrum, and improved photocatalytic activity for the water reduction compared to the previously developed quaternary system was achieved.

2 Experimental Section

2.1 Powder Synthesis by GRN

The powder samples of the system $Li_{1-x}Zn_xGe_{2-x}Ga_xN_3$ were synthesized by using the GRN method.[8,17,31–39] The oxide starting materials were prepared by simple wet mixing of Li_2CO_3 (FUJIFILM Wako Pure Chemical Co., 99%), ZnO (Sigma-Aldrich Co., no. 544906), GeO_2 (Sigma-Aldrich Co., 99.99%), and Ga_2O_3 (Sigma-Aldrich Co., 99.99%) powders. The content of ZnO in the starting composition was 3 times the stoichiometric quantity, as has been optimized previously.[17] The raw powder mixture of ∼0.3–0.4 g was loaded in an alumina boat and set in a horizontal alumina tube furnace (inner diameter of 24 mm). The sample was subsequently heated to the reaction temperature of 900°C at a ramp rate of 8.33°C/min in an NH_3–1.5 vol% CH_4 gas mixture, introduced at a constant flow rate of 0.13 SLM. The optimized holding time varied as follows: 2.5 h ($x = 0$), 3 h ($x = 0.05$), 3.5 h ($x = 0.10$), 5 h ($x = 1$), 5.5 h ($x = 0.20$), and 6 h ($x = 0.50$–0.90). After the predetermined holding time, the sample was furnace cooled in an NH_3 atmosphere with an average cooling rate of 20°C/min. (**Caution!** *The NH_3-containing exhaust gas should be absorbed by an acid trap or thermally decomposed by a subfurnace. The sample should be removed from the furnace after sufficient purging with an inert gas.*)

2.2 Characterization

The phase composition of the synthesized powders was analyzed by XRD using Cu Kα_1 radiation operated at 45 kV and 200 mA (SmartLab, Rigaku). The Rietveld refinement of the XRD data was conducted using the program RIETAN-FP.[40] The neutron diffraction pattern of $LiGe_2N_3$ was acquired by the TOF neutron powder diffractometer, BL20 iMATERIA, located at the pulsed-spallation neutron source in the Materials and Life Science Experimental Facility of the Japan Proton Accelerator Research Complex with 400 kW beam power. The pattern was collected at room temperature using the 90 degree bank with a resolution of $\Delta d/d = 0.5\%$ for $d = 0.255$–7.2 Å. The Rietveld refinement of the neutron powder diffraction pattern was conducted using the program Z-Rietveld.[41] The definitions of the reliability factors for refinement are as described by Young.[42] The bond valence sum values at the (Li,Zn,Ge,Ga) mixed occupancy sites were calculated according to the weighted long-range bond valence sum,[43] and the bond valence parameters were taken from the work by Brese and O'Keeffe.[44] The cationic compositions of the synthesized powders were analyzed by inductively coupled plasma optical emission spectrometry (ICP-OES; SPS3520UV-DD, Hitachi High-Tech Science Co.). Nitrogen and oxygen contents were analyzed by the thermal conductimetric method and infrared absorption, respectively (TC-436AR, LECO Co.). The specific surface area and the equivalent particle size of the powders were measured by the single-point Brunauer–Emmett–Teller (BET) method (FlowSorb III, Micromeritics). The ^{71}Ga magic-angle spinning (MAS) NMR measurement was conducted at 18.8 T using a JEOL ECA 800 spectrometer equipped with a home-made 3.2 mm MAS probe spinning at ca. 20 kHz. The Larmor frequency at 18.8 T was 244.12 MHz for ^{71}Ga. Spectra were acquired by 720–12200 scans using the single

pulse sequence with a 30° pulse of 1 μs and a relaxation delay of 20 s, and were referenced to 0 ppm for a 1.0 M aqueous $Ga(NO_3)_3$ solution. The diffuse reflectance spectrum of the samples was measured with a spectrophotometer (V-650, Jasco), by referring to the Spectralon reflectance standard. Photoluminescence (PL) spectra were measured at room temperature using a spectrofluorometer (FP-8500, Jasco).

2.3 Photocatalytic Reactions

The photocatalytic test reactions were carried out by using a top irradiation-type cell connected to a closed gas circulation system, as described in our previous studies.[8,17,38] The RuO_2 cocatalyst was loaded to the powder samples by impregnation from a $RuCl_3$ (FUJIFILM Wako Pure Chemical Co., 99.9%) ethanol solution, followed by the calcination in air at 400°C for 4 h. Photocatalytic H_2 evolution was examined with ∼0.22 g of the 2 wt% RuO_2-loaded samples dispersed in 200 mL of deionized water containing 10 vol % of methanol as an electron donor. O_2 evolution was evaluated in an aqueous silver nitrate solution (0.01 M) without loading the cocatalyst. The reaction cell was irradiated by UV–visible light using a 300-W Xe lamp (PE300BF, Excelitas Technologies Co.). An air mass filter (AM1.5G, Asahi Spectra Co.) was used for irradiation of the solar spectrum. The external quantum efficiency was measured by using a bandpass filter of 380 nm (MZ0380, Ashahi Spectra Co.), and the number of incident photons was predetermined by using a photodiode sensor (PD300-UV, Ophir Optronics Solutions Ltd.). The amounts of H_2 and O_2 evolved were measured using on-line gas chromatography (GC-8A, Shimadzu).

3 Results and Discussion

3.1 Synthesis and Crystal Structure

The main physicochemical properties of the $Li_{1-x}Zn_xGe_{2-x}Ga_xN_3$ powder samples synthesized are summarized in Table 1. Completion of the reduction–nitridation reaction was confirmed by weight-loss measurements for each run, and the holding time required for complete nitridation ranged from 2.5 h for $x = 0$ to 6 h for $x = 0.50$–0.90. The compositional deviations for each element, with regard to the total cation number of 3, were found to be less than 2.3% by the ICP-OES analysis. The analyzed nitrogen contents (C_N) were in fair agreement with the expected values of 16.83–21.64 wt%. The impurity oxygen contents (C_O) were found to increase from 1.21 wt % for $x = 0$ to 2.66 wt% for $x = 1$, which is attributable to the marked increase of the specific surface area (S_{BET}) from 3.3 to 13.4 m^2/g. The introduction of Li_2CO_3 with the melting point of 724°C[45] might promote transient liquid-phase formation in the reaction system, resulting in the decrease of the specific surface area in the lower x (Li rich) region. The corresponding particle size (D_{BET}) decreased from 0.38 μm for $x = 0$ to 0.07 μm for $x = 1$.

The crystal structure of the end member $LiGe_2N_3$ is shown in Figure 1. $LiGe_2N_3$ is isostructural with $NaGe_2N_3$, possessing a cation-ordered superlattice of wurtzite with the space group $Cmc2_1$.[46] This orthorhombic lattice has relationships $a \simeq 3a_w$, $b \simeq \sqrt{3}a_w$, $c \simeq c_w$ (suffix "w" stands for wurtzite), and consists of N–$LiGe_3$ and N–Li_2Ge_2 tetrahedra in the ratio of 2:1 without satisfying the local octet rule. As seen in the figures, Ge–N_4 tetrahedra tilt to accommodate larger Li–N_4 tetrahedra. The tilting of Ge–N_4 also causes a noticeable decrease of the parameter $\epsilon = 2c/(a/3 + b/\sqrt{3})$, corresponding to the c_w/a_w ratio, from the value of 1.633 for the ideal wurtzite structure.

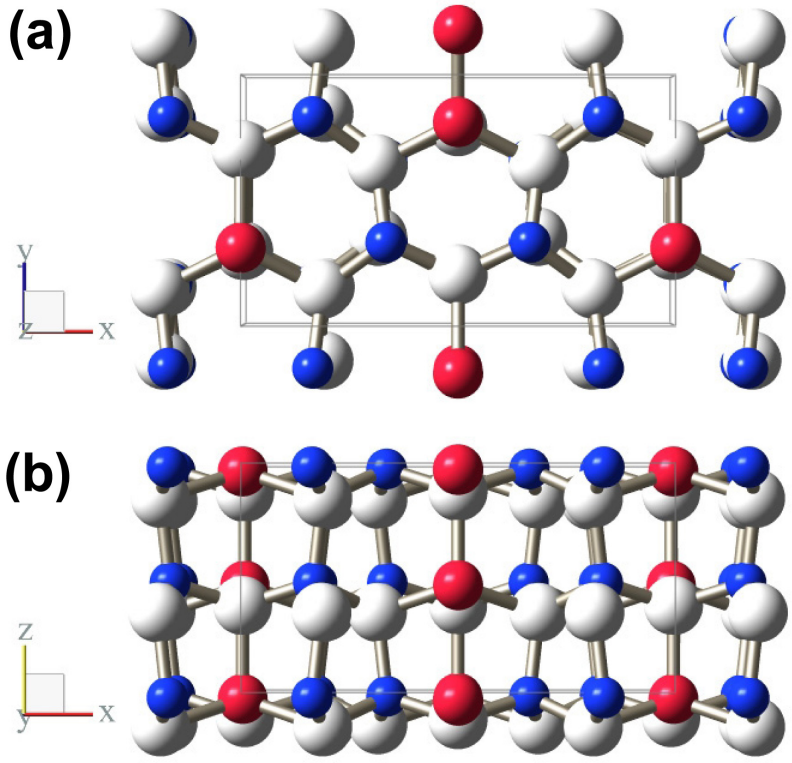

Figure 1: Crystal structure of $LiGe_2N_3$ ($Cmc2_1$) viewed along the directions of (a) [001], and (b) [010]. Li, Ge, and N atoms are represented by red, blue, and white spheres, respectively.

Table 1: Physicochemical Properties of the Synthesized $Li_{1-x}Zn_xGe_{2-x}Ga_xN_3$ Powders

x	cationic ratio[a] Li	Zn	Ge	Ga	C_N (wt %)	C_O (wt %)	S_{BET} (m^2/g)	D_{BET} (μm)	E_g (eV)
0	1.030(14)		1.970(8)		20.04(7)	1.21(2)	3.3	0.38	4.16
0.05	0.980(8)	0.075(1)	1.893(6)	0.052(1)	19.68(8)	1.21(1)	4.3	0.28	3.81
0.10	0.916(14)	0.139(1)	1.840(12)	0.105(1)	19.37(10)	1.36(3)	4.9	0.25	3.72
0.20	0.826(2)	0.214(1)	1.752(2)	0.208(1)	18.99(6)	1.09(3)	5.6	0.21	3.54
0.50	0.506(7)	0.531(2)	1.444(9)	0.519(7)	17.88(3)	1.24(9)	6.5	0.17	3.27
0.80	0.224(2)	0.823(1)	1.133(7)	0.820(2)	16.31(3)	1.83(5)	8.8	0.12	3.16
0.90	0.119(1)	0.926(2)	1.032(2)	0.923(2)	15.79(1)	2.09(5)	9.8	0.10	3.10
1		1.005(2)	0.972(1)	1.023(1)	15.32(4)	2.66(1)	13.4	0.07	3.03

[a]Normalized against the total of 3.

No satisfactorily precise crystal structure data for $LiGe_2N_3$ have been reported up to now, mainly due to the uncertain atomic coordinates obtained by powder XRD.[30] In the current work, we could precisely determine the atomic coordinates for the lighter elements of Li and N, by conducting TOF neutron powder diffraction experiments for the single phase $LiGe_2N_3$ synthesized. The plot of Rietveld refinement pattern is presented in Figure 2, and the obtained crystallographic data and the relevant bond lengths are provided in Tables 2 and 3, respectively. The refinement converged with $R_{wp} = 4.25\%$, $S = 4.36$ ($R_e = 0.98\%$), $R_B = 1.71\%$, and $R_F = 2.23\%$. The parameter ϵ derived from the refined lattice constants was 1.581, markedly lower than 1.624 for another end member of $ZnGeGaN_3$ with the wurtzite structure.[17,39] The variation between the mean tetrahedral Li–N bond distance of 2.119 Å and the fifth closest Li–N distance (2.971 Å) was as large as

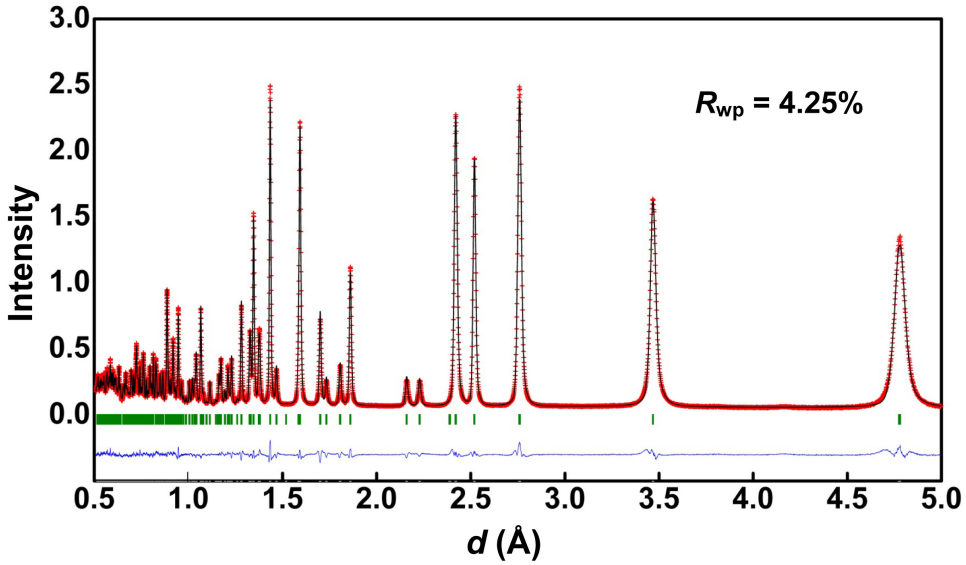

Figure 2: Rietveld refinement pattern of the TOF neutron powder diffraction data for the synthesized $LiGe_2N_3$.

40.2%, and thus the Li ions should be definitely regarded as tetracoordinated in $LiGe_2N_3$. The bond valence sum values were calculated to be 1.02 for Li and 4.32 for Ge, comparable to each formal valency, indicating a complete cation ordering attained in the synthesized $LiGe_2N_3$.

Figure 3 shows the XRD patterns of the synthesized $Li_{1-x}Zn_xGe_{2-x}Ga_xN_3$ samples with the various x values. In our previous work,[39] we have revealed by the TOF neutron powder diffraction experiment that the end member $ZnGeGaN_3$ possesses a fully cation-disordered wurtzite structure. Thus, the cation arrangement in the current $Li_{1-x}Zn_x$-$Ge_{2-x}Ga_xN_3$ system is expected to exhibit a transition from the completely ordered state at $x = 0$ to the fully disordered state at $x = 1$. The diffraction peaks of 110/200 and 111, clearly observed at $x = 0$, are typical superlattice satellite peaks of the $Cmc2_1$ structure, resulting from the large difference of the electron density between Li and Ge. These superlattice peaks showed a monotonic decrease of the intensity with the increase of x

Table 2: Refined Crystallographic Data[a] for $LiGe_2N_3$ Determined by TOF neutron powder diffraction

atom	site	SOF	x	y	z	B (Å^2)
Li	4a	1	0	0.3120(6)	0.9683(3)	2.93(4)
Ge	8b	1	0.16583(5)	0.83322(10)	0.97963(1)	0.395(3)
N(1)	8b	1	0.18729(3)	0.85378(7)	0.34859(2)	0.405(2)
N(2)	4a	1	0	0.29661(5)	0.37897(3)	0.405(2)

[a]Space group $Cmc2_1$ (No. 36), $a = 9.55210(5)$ Å, $b = 5.52312(3)$ Å, $c = 5.03901(1)$ Å, $V = 265.845(2)$ Å^3, $Z = 4$, reliability factors: $R_{\rm wp} = 4.25\%$, $R_{\rm B} = 1.71\%$, $R_F = 2.23\%$.

Table 3: Tetrahedral Li–N and Ge–N Bond Distances for $LiGe_2N_3$

Li–N distances (Å)		Ge–N distances (Å)	
Li–N(1)	2.098(1) × 2	Ge–N(1)	1.8739(1)
Li–N(2)	2.071(1)	Ge–N(1)	1.8619(6)
Li–N(2)	2.208(3)	Ge–N(1)	1.8631(7)
		Ge–N(2)	1.8112(4)
mean	2.119(1)	mean	1.8525(3)

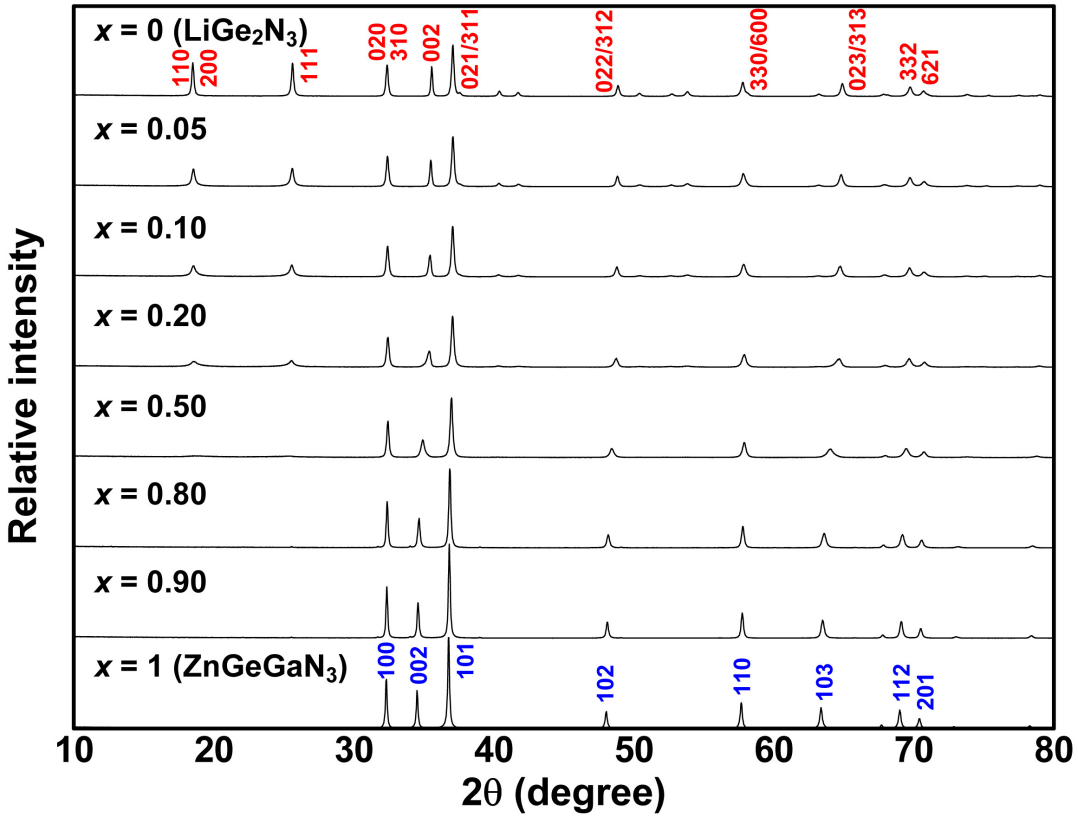

Figure 3: XRD patterns of the synthesized $Li_{1-x}Zn_xGe_{2-x}Ga_xN_3$ with the various x values.

and almost disappeared at $x = 0.50$, which might result from the occupation of much heavier Zn at the Li site, as well as from the progression of the cation disorder. Table 4 lists the main structural parameters for the penternary compositions, obtained through the Rietveld refinement of the XRD data. The refinement was conducted based on the orthorhombic $Cmc2_1$ model with the general formula $(Li_{1-x}Zn_x)(1)_{1-i}(Ge_{1-x/2}Ga_{x/2})(2)_i$-$(Ge_{1-x/2}Ga_{x/2})(1)_{2-i}(Li_{1-x}Zn_x)(2)_iN_3$, where i denotes the inversion parameter of the original Li (4a) and Ge (8b) sites, i.e., (Ge,Ga)(2) and (Li,Zn)(2) stand for the antisites. The fully cation-disordered state corresponds to $i = 2/3$, and the degree of disorder is defined as $3i/2$. The lattice constant c, as well as the parameter ϵ tended to increase with

Table 4: Structural Parameters for the $Li_{1-x}Zn_xGe_{2-x}Ga_xN_3$ Penternary Compositions, Obtained through the XRD Rietveld Refinement

x	a (Å)	b (Å)	c (Å)	ϵ	i	degree of disorder (%)
0.05	9.5473(4)	5.5244(2)	5.0505(1)	1.585	0.109(3)	16.4(5)
0.10	9.5460(7)	5.5209(4)	5.0591(1)	1.589	0.195(3)	29.3(5)
0.20	9.5404(9)	5.5183(5)	5.0698(2)	1.593	0.319(4)	47.9(6)
0.50	9.5277(2)	5.5233(2)	5.1286(1)	1.612	0.581(9)	87.2(14)
0.80	9.5547(3)	5.5252(2)	5.16898(6)	1.622	-	-
0.90	9.5622(2)	5.5284(1)	5.17803(4)	1.623	-	-

x and showed marked increases at around $x = 0.50$, where the superlattice satellite peaks almost disappear, suggesting that the tilting of the (Ge,Ga)–N_4 tetrahedra became less pronounced due to the less ordered distribution of larger (Li,Zn) and smaller (Ge,Ga) ions. The values of ϵ with $x > 0.50$ were almost comparable to 1.624 in $ZnGeGaN_3$, indicating that the cation arrangement is practically disordered in this compositional region. The inversion parameter i was determined with sufficient precision by the refinement of the site occupancy factor (SOF) of the (Ge,Ga)(2) site, and the resultant degree of disorder increased from 16.4% at $x = 0.05$ to 47.9% at $x = 0.20$, and reached as high as ∼87% at $x = 0.50$.

The appropriateness of the proposed penternary model and the derived structural parameters are also supported by the ^{71}Ga MAS NMR spectroscopy results presented in Figure 4. At the composition of $x = 0.05$, only a single resonance centered at ∼290 ppm was observed, suggesting a selective occupancy of Ga at the Ge site, consistent

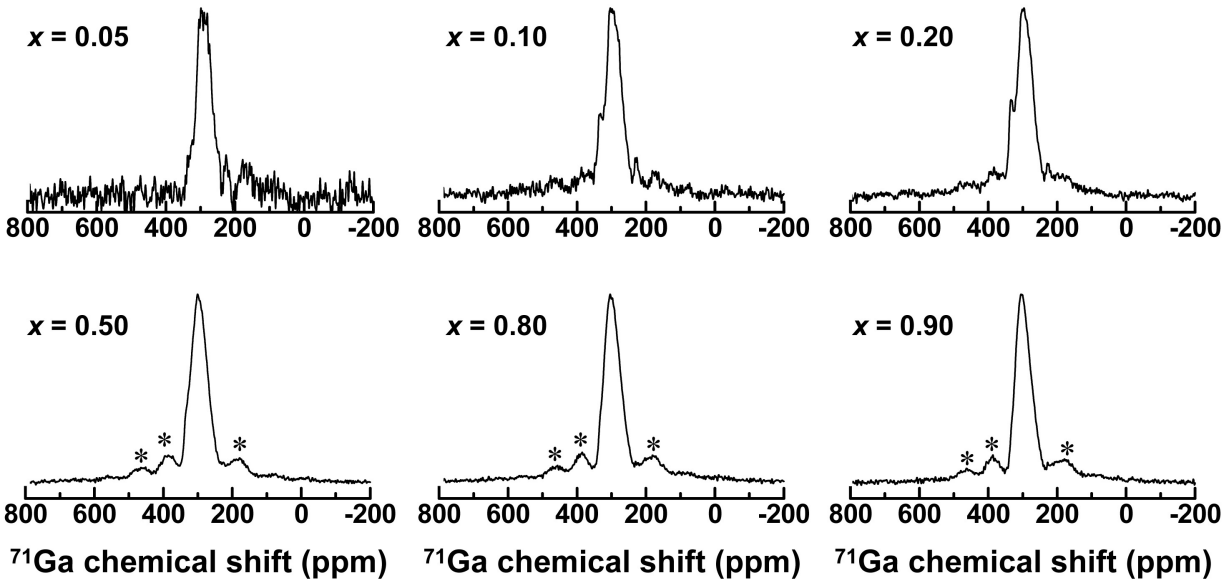

Figure 4: ^{71}Ga MAS NMR spectra of the synthesized $Li_{1-x}Zn_xGe_{2-x}Ga_xN_3$. Asterisks indicate spinning sidebands.

with the rather low disorder degree of 16.4%. With the increase of x, Ga ions tended to also occupy the larger (Li,Zn) site, as indicated by a shoulder peak at ∼335 ppm observed with the compositions of $x = 0.10$ and 0.20. It should be noted that the larger chemical shift of the shoulder peak implies weaker shielding with the ligand, i.e., longer nitrogen coordination distances at the (Li,Zn) site. These two peaks were nearly unified into a single band at $x = 0.50$, where the degree of disorder reached about 90%, and the compositions with $x = 0.80$ and 0.90 exhibited an essentially single peak at ∼300 ppm, indicating the indistinguishable coordination environment around the cations in the disordered wurtzite structure. Figure 5 shows the result of XRD Rietveld refinement for the sample with $x = 0.90$, conducted based on the disordered wurtzite structure ($P6_3mc$). The refined crystallographic data and the (Li,Zn,Ge,Ga)–N bond lengths are provided in Tables 5 and 6, respectively. The refinement sufficiently converged with the

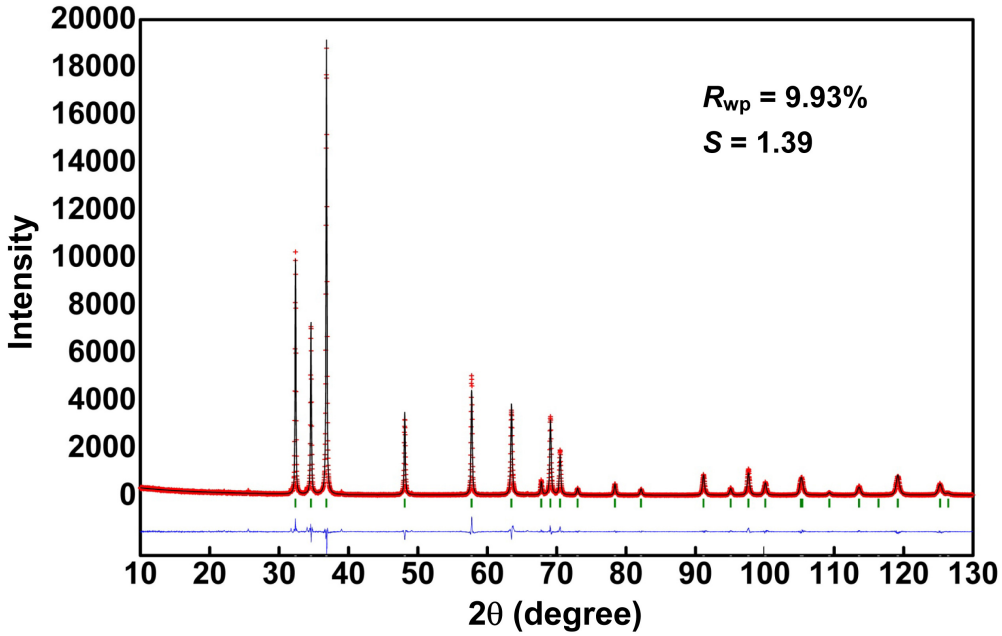

Figure 5: XRD Rietveld refinement pattern of the synthesized $Li_{1-x}Zn_xGe_{2-x}Ga_xN_3$ with $x = 0.90$.

reliability factors of $R_{\mathrm{wp}} = 9.93\%$, $S = 1.39$, $R_{\mathrm{B}} = 2.48\%$, and $R_F = 1.51\%$, proving the expected complete disorder of the cation sublattice. The bond valence sum derived from the obtained (Li,Zn,Ge,Ga)–N bond distance data was 2.90, in reasonable agreement with the average valency of 3.

Table 5: Refined Crystallographic Data[a] for the $x = 0.90$ Sample with the Composition $Li_{0.0333}Zn_{0.3000}Ge_{0.3667}Ga_{0.3000}N$

atom	site	SOF	x	y	z	B (Å^2)
Li	2b	0.0333	1/3	2/3	0	0.33(1)
Zn	2b	0.3	1/3	2/3	0	0.33(1)
Ge	2b	0.3667	1/3	2/3	0	0.33(1)
Ga	2b	0.3	1/3	2/3	0	0.33(1)
N	2b	1	1/3	2/3	0.3824(6)	0.39(7)

[a]Space group $P6_3mc$ (No. 186), $a = 3.18955(2)$ Å, $c = 5.17791(4)$ Å, $V = 45.6189(6)$ Å^3, $Z = 2$, reliability factors: $R_{wp} = 9.93\%$, $R_B = 2.48\%$, $R_F = 1.51\%$.

Table 6: (Li,Zn,Ge,Ga)–N Bond Distances for $Li_{0.0333}Zn_{0.3000}Ge_{0.3667}Ga_{0.3000}N$

tetrahedral (Li,Zn,Ge,Ga)–N distances (Å)	
(Li,Zn,Ge,Ga)–N	1.940(1) × 3
	1.980(3)
mean	1.950(1)

3.2 Optical Properties

The band gap energy (E_g) estimated from the Tauc plots of $(\alpha h\nu)^2$ vs $h\nu$ is shown in Figure 6(a), where the pseudo absorption coefficient α was obtained by Kubelka–Munk transformation of the diffuse-reflectance spectra. The end member $LiGe_2N_3$, as well as $ZnGeGa_2N_4$ ($x = 0.5$ in $Zn_{1-x}Ge_{1-x}Ga_{2x}N_2$) were expected to possess direct transition.[28,30] The band gap of $LiGe_2N_3$ obtained from the linear plot was located in the UV region of 4.16 eV (298 nm), while E_g of the penternary compositions successively shifted to lower energy region down to 3.03 eV (409 nm) for $x = 1$, showing promising responsivity to the solar spectrum. The dependence of E_g on the composition x is also shown in Figure 6(b). The E_g value varied with obvious deviation from Vegard's law, suggesting the contribution of the cation disorder discussed earlier. The least-squares fitting gives a nominal bowing parameter of 1.57(13) eV.

Figure 7 shows the PL excitation and emission spectra of the synthesized $Li_{1-x}Zn_xGe_{2-x}Ga_xN_3$ powders. The penternary compositions containing Zn and Ga exhibited yellow-orange broadband emission as has been observed for the $Zn_{1-x}Ge_{1-x}Ga_{2x}N_2$ system,[8,17] while the end member $LiGe_2N_3$ was completely nonluminescent under the excitation of $\lambda \geq 200$ nm. The excitation peak redshifted with the increase of x in the range of ∼300–410 nm, reflecting the decrease of the E_g value with x.

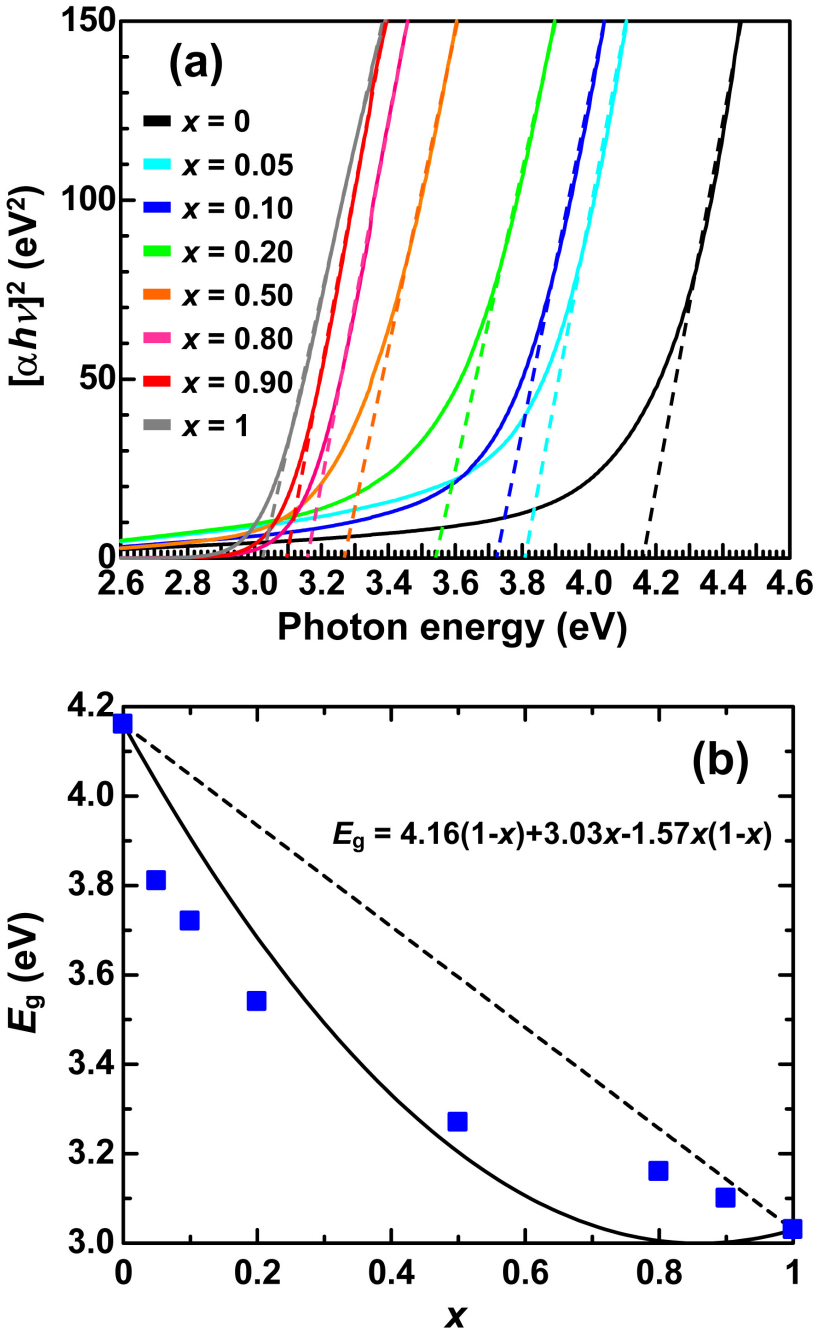

Figure 6: (a) plots of $(\alpha h\nu)^2$ vs $h\nu$ showing the E_g values, and (b) dependence of E_g on the value of x for the synthesized $Li_{1-x}Zn_xGe_{2-x}Ga_xN_3$.

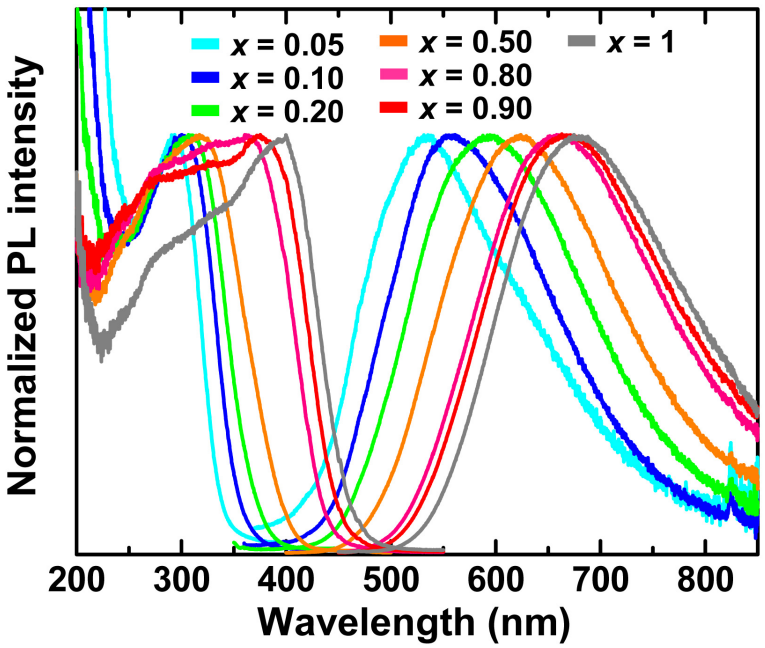

Figure 7: PL excitation and emission spectra of the synthesized $Li_{1-x}Zn_xGe_{2-x}Ga_xN_3$.

3.3 Photocatalytic Activity

Table 7 lists the photocatalytic activities of the synthesized $Li_{1-x}Zn_xGe_{2-x}Ga_xN_3$ powder samples for the water reduction and oxidation reactions, observed under the simulated solar-light irradiation (AM1.5G). The end member $LiGe_2N_3$ showed almost null activities for both the H_2 and O_2 evolution, as expected from the large E_g value of 4.16 eV (298 nm). The penternary compositions, possessing sensitivities to the solar spectrum with $E_g \leq 3.81$ eV (≥ 325 nm), exhibited a gradual increase of the H_2 evolution rate with the increase of x, showing a maximum of 59.0 μmol/h at $x = 0.80$. The marked decrease of the H_2 evolution rate with $x > 0.80$ implies that the further decrease of the band gap might result in an insufficiently low overpotential exerting on the reduction of H^+ to H_2. On the other hand, the evolution rate of O_2 showed a monotonic increase from 3.1 μmol/h for $x = 0.05$ to 296.2 μmol/h for $x = 1$, indicating that the water oxidation reaction might be promoted primarily by the increased sensitivity to the solar spectrum, considering the less pronounced increase of the specific surface area (Table 1). Figure 8 presents the time dependence of the H_2 evolution by water reduction, performed with the $x = 0.80$ sample up to a reaction period of 48 h. The H_2 evolution proceeded with no detectable formation of N_2 resulting from degradation, and the total H_2 produced amounted to 1.676 mmol. After 48 h operation, the external quantum efficiency at 380 nm excitation was measured to be 2.1%.

Table 7: Photocatalytic Activities of the $Li_{1-x}Zn_xGe_{2-x}Ga_xN_3$ Powder Samples for Water Reduction and Oxidation under Simulated Solar Light Irradiation (AM1.5G)

	activity (μmol/h)	
x	H_2[a]	O_2[b]
0	0.1	0.0
0.05	0.3	3.1
0.10	2.8	8.1
0.20	15.6	23.7
0.50	51.5	110.5
0.80	59.0	194.3
0.90	8.4	276.3
1	10.1	296.2

[a]Average evolution rate of 5 h run.
[b]Evolution rate of 1 h run.

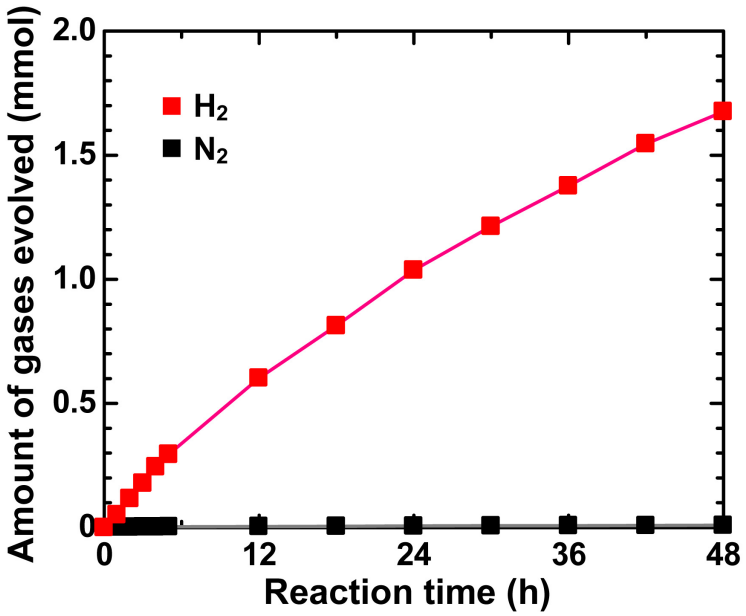

Figure 8: Time dependence of photocatalytic H_2 evolution by water reduction performed with the synthesized $Li_{1-x}Zn_xGe_{2-x}Ga_xN_3$ ($x = 0.80$) powder, under simulated solar-light irradiation.

4 Conclusions

A new penternary wurtzitic nitride system $Li_{1-x}Zn_xGe_{2-x}Ga_xN_3$ ($0 \leq x \leq 1$) has been developed by the solid-solution formation between $LiGe_2N_3$ and $ZnGeGaN_3$. Fairly stoichiometric fine powder samples with the particle size of 0.07–0.38 μm were successfully synthesized by the GRN reaction at 900°C. The end member $LiGe_2N_3$ possessed a relatively wide band gap of 4.16 eV, while the E_g value of the developed penternary system varied in a broad range of 3.81–3.10 eV (325–400 nm), showing the promising responsivity to the solar spectrum. The crystal structure of $LiGe_2N_3$ was precisely determined by the Rietveld refinement of the TOF neutron powder diffraction pattern, and the obtained bond valence sum data indicated the complete cation ordering attained by the current synthesis method. The expected structural evolution from the completely ordered $LiGe_2N_3$ to the fully disordered $ZnGeGaN_3$ was analyzed quantitatively with a penternary $Cmc2_1$ model considering the inversion of the (Li,Zn) and (Ge,Ga) sites. The estimated degree of disorder reached ∼50% at $x = 0.20$ and ∼90% at $x = 0.50$, beyond which the structure transformed to the fully disordered $P6_3mc$ phase. The observed order-disorder transition was also confirmed by the results of ^{71}Ga MAS NMR spectroscopy, which clearly showed the gradual convergence of two peaks, originating from the $Cmc2_1$ structure, into a single resonance with $x \geq 0.50$. The synthesized $Li_{1-x}Zn_xGe_{2-x}Ga_xN_3$ powders exhibited photocatalytic activities for the water reduction and oxidation reactions under the solar-light irradiation, and the sample with $x = 0.80$ showed a maximum H_2 evolution rate of 59.0 μmol/h, while retaining a relatively high O_2 evolution rate of 194.3 μmol/h. With the $x = 0.80$ sample, stable solar hydrogen generation of up to 48 h was demonstrated, with the amount of H_2 produced reaching 1.676 mmol and the external quantum efficiency of

2.1% at 380 nm.

Acknowledgments. We are grateful to Mr. S. Takenouchi, formerly of NIMS for the chemical analyses, and to Mr. K. Deguchi and Mr. S. Ohki of NIMS for the NMR measurements. Thanks are also extended to Prof. A. Hoshikawa of Ibaraki University for the neutron diffraction experiments. The neutron experiment was performed under a user program (Proposal No. 2017B0081). This work was supported by JSPS KAKENHI, grant no. 21K04913 (T. Suehiro).

References

(1) Stratulat, A.-M.; Tantardini, C.; Azizi, M.; Altalhi, T.; Levchenko, S. V.; Yakobson, B. I. Electronic Properties of $Zn_2V_{1-x}Nb_xN_3$ Alloys to Model Novel Materials for Light-Emitting Diodes. *J. Phys. Chem. Lett.* **2023**, *14*, 9118–9125.

(2) Hassine, S.; Farkad, O.; Elfatouaki, F.; Takassa, R.; El Mouncharih, A.; Choukri, O.; Ouahdani, A.; Ibnouelghazi, E. A.; Abouelaoualim, D. Electronic and optical properties of bulk Zn_2VN_3 ternary nitride: First-principles investigation. *Mater. Sci. Semicond. Process.* **2023**, *166*, 107725.

(3) Zhuk, S.; Wieczorek, A.; Sharma, A.; Patidar, J.; Thorwarth, K.; Michler, J.; Siol, S. Combinatorial Reactive Sputtering with Auger Parameter Analysis Enables Synthesis of Wurtzite Zn_2TaN_3. *Chem. Mater.* **2023**, *35*, 7069–7078.

(4) Rom, C. L.; Smaha, R. W.; Melamed, C. L.; Schnepf, R. R.; Heinselman, K. N.; Mangum, J. S.; Lee, S.-J.; Lany, S.; Schelhas, L. T.; Greenaway, A. L.; Neilson, J. R.; Bauers, S. R.; Tamboli, A. C.; Andrew, J. S. Combinatorial Synthesis of Cation-Disordered Manganese Tin Nitride $MnSnN_2$ Thin Films with Magnetic and Semiconducting Properties. *Chem. Mater.* **2023**, *35*, 2936–2946.

(5) Dernek, O.; Lambrecht, W. R. L. Quaternary $MgSiN_2$–GaN alloy semiconductors for deep UV applications. *Phys. Rev. B* **2022**, *106*, 235122.

(6) Zakutayev, A.; Bauers, S. R.; Lany, S. Experimental Synthesis of Theoretically Predicted Multivalent Ternary Nitride Materials. *Chem. Mater.* **2022**, *34*, 1418–1438.

(7) Greenaway, A. L.; Ke, S.; Culman, T.; Talley, K. R.; Mangum, J. S.; Heinselman, K. N.; Kingsbury, R. S.; Smaha, R. W.; Gish, M. K.; Miller, E. M.; Persson, K. A.; Gregoire, J. M.; Bauers, S. R.; Neaton, J. B.; Tamboli, A. C.; Zakutayev, A. Zinc Titanium Nitride Semiconductor toward Durable Photoelectrochemical Applications. *J. Am. Chem. Soc.* **2022**, *144*, 13673–13687.

(8) Suehiro, T.; Tansho, M.; Ishigaki, T.; Shimizu, T. Quaternary Wurtzitic Nitrides $(1-x)ZnGeN_2$–$2x$GaN (x = 0.02, 0.05): Disorder-Induced Band-Gap Narrowing and Potentiality as a Solar-Active Photocatalyst. *Inorg. Chem.* **2021**, *60*, 1542–1549.

(9) Ogura, M.; Han, D.; Pointner, M. M.; Junkers, L. S.; Rudel, S. S.; Schnick, W.; Ebert, H. Electronic properties of semiconducting Zn(Si,Ge,Sn)N_2 alloys. *Phys. Rev. Mater.* **2021**, *5*, 024601.

(10) Zhuk, S.; Kistanov, A. A.; Boehme, S. C.; Ott, N.; La Mattina, F.; Stiefel, M.; Kovalenko, M. V.; Siol, S. Synthesis and Characterization of the Ternary Nitride Semiconductor Zn_2VN_3: Theoretical Prediction, Combinatorial Screening, and Epitaxial Stabilization. *Chem. Mater.* **2021**, *33*, 9306–9316.

(11) Zakutayev, A. Synthesis of Zn_2NbN_3 ternary nitride semiconductor with wurtzite-derived crystal structure. *J. Phys. Condens. Matter* **2021**, *33*, 354003.

(12) Schnepf, R. R.; Cordell, J. J.; Tellekamp, M. B.; Melamed, C. L.; Greenaway, A. L.; Mis, A.; Brennecka, G. L.; Christensen, S.; Tucker, G. J.; Toberer, E. S.; Lany, S.; Tamboli, A. C. Utilizing Site Disorder in the Development of New Energy-Relevant Semiconductors. *ACS Energy Lett.* **2020**, *5*, 2027–2041.

(13) Jayatunga, B. H. D.; Karim, M. R.; Lalk, R. A.; Ohanaka, O.; Lambrecht, W. R. L.; Zhao, H.-P.; Kash, K. Metal-Organic Chemical Vapor Deposition of $ZnGeGa_2N_4$. *Cryst. Growth Des.* **2020**, *20*, 189–196.

(14) Melamed, C. L.; Tellekamp, M. B.; Mangum, J. S.; Perkins, J. D.; Dippo, P.; Toberer E. S.; Tamboli, A. C. Blue-Green Emission from Epitaxial yet Cation-Disordered $ZnGeN_{2-x}O_x$. *Phys. Rev. Mater.* **2019**, *3*, 051602(R).

(15) Adamski, N. L.; Zhu, Z.; Wickramaratne, D.; Van de Walle, C. G. Strategies for *p*-type Doping of $ZnGeN_2$. *Appl. Phys. Lett.* **2019**, *114*, 032101.

(16) Wang, J.; Asakura, Y.; Yin, S. Preparation of $(Zn_{1+x}Ge)(N_2O_x)$ nanoparticles with enhanced NO_x decomposition activity under visible light irradiation by nitridation of Zn_2GeO_4 nanoparticles designed precisely. *Nanoscale* **2019**, *11*, 20151–20160.

(17) Suehiro, T.; Tansho, M.; Shimizu, T. Quaternary Wurtzitic Nitrides in the System $ZnGeN_2$–GaN: Powder Synthesis, Characterization, and Potentiality as a Photocatalyst. *J. Phys. Chem. C* **2017**, *121*, 27590–27596.

(18) Han, L.; Kash, K.; Zhao, H. Designs of Blue and Green Light-Emitting Diodes Based on Type-II InGaN-$ZnGeN_2$ Quantum Wells. *J. Appl. Phys.* **2016**, *120*, 103102.

(19) Shang, M.; Wang, J.; Fan, J.; Lian, H.; Zhang, Y.; Lin, J. $ZnGeN_2$ and $ZnGeN_2$:Mn^{2+} Phosphors: Hydrothermal-Ammonolysis Synthesis, Structure and Luminescence Properties. *J. Mater. Chem. C* **2015**, *3*, 9306–9317.

(20) Veal, T. D.; Feldberg, N.; Quackenbush, N. F.; Linhart W. M.; Scanlon, D. O.; Piper, L. F. J.; Durbin, S. M. Band Gap Dependence on Cation Disorder in $ZnSnN_2$ Solar Absorber. *Adv. Energy Mater.* **2015**, *5*, 1501462.

(21) Lahourcade, L.; Coronel, N. C.; Delaney, K. T.; Shukla, S. K.; Spaldin, N. A.; Atwater, H. A. Structural and Optoelectronic Characterization of RF Sputtered $ZnSnN_2$. *Adv. Mater.* **2013**, *25*, 2562–2566.

(22) Feldberg, N.; Aldous, J. D.; Linhart, W. M.; Phillips, L. J.; Durose, K.; Stampe, P. A.; Kennedy, R. J.; Scanlon, D. O.; Vardar, G.; Field, R. L., III; Jen, T. Y.; Goldman, R. S.; Veal, T. D.; Durbin, S. M. Growth, Disorder, and Physical Properties of $ZnSnN_2$. *Appl. Phys. Lett.* **2013**, *103*, 042109.

(23) Punya, A.; Lambrecht, W. R. L. Band Offsets between $ZnGeN_2$, GaN, ZnO, and $ZnSnN_2$ and Their Potential Impact for Solar Cells. *Phys. Rev. B* **2013**, *88*, 075302.

(24) Zhang, Q.-H.; Wang, J.; Yeh, C.-W.; Ke, W.-C.; Liu, R.-S.; Tang, J.-K.; Xie, M.-B.; Liang, H.-B.; Su, Q. Structure, Composition, Morphology, Photoluminescence and Cathodoluminescence Properties of $ZnGeN_2$ and $ZnGeN_2$:Mn^{2+} for Field Emission Displays. *Acta Mater.* **2010**, *58*, 6728–6735.

(25) Jaroenjittichai, A. P.; Lyu, S.; Lambrecht, W. R. L. Erratum: Band Offsets between $ZnGeN_2$, GaN, ZnO, and $ZnSnN_2$ and Their Potential Impact for Solar Cells [Phys. Rev. B 88, 075302 (2013)]. *Phys. Rev. B* **2017**, *96*, 079907(E).

(26) Wintenberger, M.; Maunaye, M.; Laurent, Y. Groupe Spatial et Ordre des Atomes de Zinc et de Germanium dans $ZnGeN_2$. *Mater. Res. Bull.* **1973**, *8*, 1049–1054.

(27) Paszkowicz, W.; Podsiadło, S.; Minikayev, R. Rietveld-Refinement Study of Aluminium and Gallium Nitrides. *J. Alloys. Compd.* **2004**, *382*, 100–106.

(28) Jayatunga, B. H. D.; Lyu, S.; Radha, S. K.; Kash, K.; Lambrecht, W. R. L. Ordering in the Mixed $ZnGeN_2$-GaN Alloy System: Crystal Structures and Band Structures of $ZnGeGa_2N_4$ from First Principles. *Phys. Rev. Mater.* **2018**, *2*, 114602.

(29) David, J.; Charlot, J. P.; Lang, J. Les nitrures doubles de lithium et de germanium. *Rev. Chim. Miner.* **1974**, *11*, 405–413.

(30) Häusler, J.; Niklaus, R.; Minár, J.; Schnick, W. Ammonothermal Synthesis and Optical Properties of Ternary Nitride Semiconductors Mg-IV-N_2 and Li-IV_2-N_3 (IV=Si, Ge). *Chem. Eur. J.* **2018**, *24*, 1686–1693.

(31) Suehiro, T.; Hirosaki, N.; Komeya, K. Synthesis and Sintering Properties of Aluminium Nitride Nanopowder Prepared by the Gas-Reduction–Nitridation Method. *Nanotechnology* **2003**, *14*, 487–491.

(32) Suehiro, T.; Hirosaki, N.; Xie, R.-J.; Mitomo, M. Powder Synthesis of Ca-α'-SiAlON as a Host Material for Phosphors. *Chem. Mater.* **2005**, *17*, 308–314.

(33) Suehiro, T.; Hirosaki, N.; Xie, R.-J.; Sakuma, K.; Mitomo, M.; Ibukiyama, M.; Yamada, S. One-Step Preparation of Ca-α-SiAlON:Eu^{2+} Fine Powder Phosphors for White Light-Emitting Diodes. *Appl. Phys. Lett.* **2008**, *92*, 191904.

(34) Suehiro, T.; Hirosaki, N.; Xie, R.-J.; Sato, T. Blue-Emitting $LaSi_3N_5$:Ce^{3+} Fine Powder Phosphor for UV-Converting White Light-Emitting Diodes. *Appl. Phys. Lett.* **2009**, *95*, 051903.

(35) Suehiro, T.; Onuma, H.; Hirosaki, N.; Xie, R.-J.; Sato, T.; Miyamoto, A. Powder Synthesis of Y-α-SiAlON and Its Potential as a Phosphor Host. *J. Phys. Chem. C* **2010**, *114*, 1337–1342.

(36) Suehiro, T.; Hirosaki, N.; Xie, R.-J. Synthesis and Photoluminescent Properties of $(La,Ca)_3Si_6N_{11}:Ce^{3+}$ Fine Powder Phosphors for Solid-State Lighting. *ACS Appl. Mater. Interfaces* **2011**, *3*, 811–816.

(37) Suehiro, T.; Xie, R.-J.; Hirosaki, N. Gas-Reduction–Nitridation Synthesis of $CaAlSiN_3:Eu^{2+}$ Fine Powder Phosphors for Solid-State Lighting. *Ind. Eng. Chem. Res.* **2014**, *53*, 2713–2717.

(38) Suehiro, T.; Tansho, M.; Shimizu, T. Na-α'-GeGaON Solid Solution Analogous to α'-SiAlON: Synthesis, Crystal Structure, and Potentiality as a Photocatalyst. *Inorg. Chem.* **2016**, *55*, 2355–2362.

(39) Suehiro, T.; Tansho, M.; Hagihala, M.; Torii, S.; Kamiyama, T.; Shimizu, T. Quaternary Nitride System $(1-x)ZnGeN_2$–$2xGaN$ ($x = 1/3$): Disordered Wurtzite Structure Revealed by Time-of-Flight Neutron Powder Diffraction. *Appl. Phys. Express* **2020**, *13*, 115503.

(40) Izumi, F.; Momma, K. Three-Dimensional Visualization in Powder Diffraction. *Solid State Phenom.* **2007**, *130*, 15–20.

(41) Oishi, R.; Yonemura, M.; Nishimaki, Y.; Torii, S.; Hoshikawa, A.; Ishigaki, T.; Morishima, T.; Mori, K.; Kamiyama, T. Rietveld Analysis Software for J-PARC. *Nucl. Instrum. Methods Phys. Res. A* **2009**, *600*, 94–96.

(42) Young, R. A. *The Rietveld Method*, Chap. 1, Oxford University Press, Oxford, 1995.

(43) Bosi, F. Bond Valence at Mixed Occupancy Sites. I. Regular Polyhedra. *Acta Crystallogr., Sect. B: Struc. Sci.* **2014**, *B70*, 864–870.

(44) Brese, N. E.; O'Keeffe, M. Bond-Valence Parameters for Solids. *Acta Crystallogr., Sect. B: Struc. Sci.* **1991**, *B47*, 192–197.

(45) Klement, W. Jr.; Cohen, L. H. Solid-Solid and Solid-Liquid Transitions in K_2CO_3, Na_2CO_3 and Li_2CO_3: Investigations to ≥ 5 kbar by Differential Thermal Analysis; Thermodynamics and Structural Correlations. *Ber. Bunsenges. Phys. Chem.* **1975**, *79*, 327–334.

(46) Guyader, J.; L'Haridon, P.; Laurent, Y.; Jacquet, R.; Roult, G. Un Nouveau Tetraedre Azote NaN_4: Preparation et Structure de $NaGe_2N_3$. *J. Solid State Chem.* **1984**, *54*, 251–255.

For Table of Contents Only

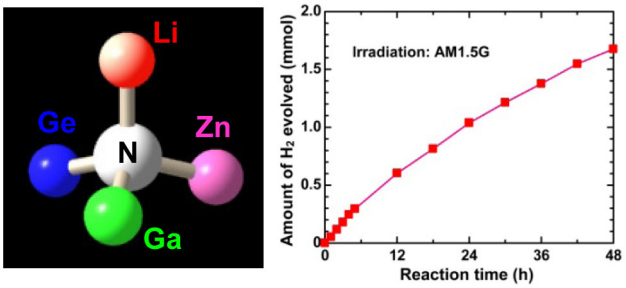

We developed a new penternary nitride system $Li_{1-x}Zn_xGe_{2-x}Ga_xN_3$ ($0 \leq x \leq 1$) by hybridizing ternary and quaternary wurtzitic nitrides, $LiGe_2N_3$ and $ZnGeGaN_3$. The synthesized $Li_{1-x}Zn_xGe_{2-x}Ga_xN_3$ exhibited promising sensitivity to the solar spectrum, and improved photocatalytic activity for the water reduction compared to the previously developed quaternary system was achieved.